Chapter 6

Reversible and Irreversible Effects in μc-Si:H

Even though highly crystalline μc-Si:H does not suffer from light induced degradation, known as Staebler-Wronski-Effect [7, 86], the particular structure properties, described in section 2.1, suggest that instabilities and metastable phenomena may also occur in this material. In particular, μc-Si:H grown at high hydrogen dilution, which yields the largest grain sizes and the highest crystalline volume fraction, shows a pronounced porosity. The existence of crack-like voids in this material facilitates the diffusion of atmospheric gases into the structure. Adsorption and/or chemical reactions, e.g. oxidation, at the column boundaries, might lead to the creation or termination of surface states and might significantly affect the electronic properties of the material.

In the following Chapter, we want to investigate and identify instability effects caused by adsorption and oxidation in μc-Si:H and want to relate them to changing structure compositions, ranging from highly crystalline porous, to highly crystalline compact and mixed phase amorphous/crystalline material.

6.1 Metastable Effects in μc-Si:H

In this section, reversible phenomena in undoped μc-Si:H with various structure compositions are identified and their investigation by the use of electron spin resonance and electrical conductivity measurements is reported.

6.1.1 Influences of Sample Preparation

Material with different structure compositions deposited on both Al and Mo substrates was prepared using VHF-PECVD and studied extensively by ESR. The

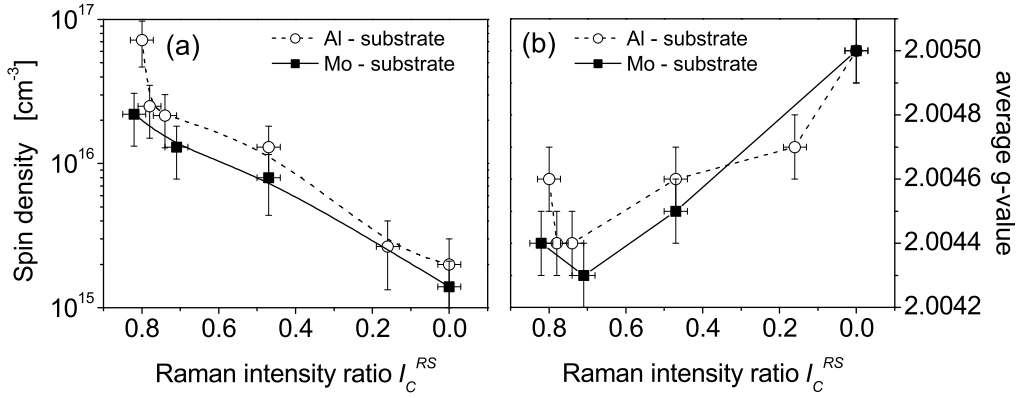

Figure 6.1: *(a) Spin density N_S of μc-Si:H powder obtained from Al substrates (★) and Mo (■). In panel (b) the corresponding g-values are plotted.*

use of these different substrates requires a different handling of the material as described in section 3.3.1. While material deposited on aluminum foil is in contact with acids, water, and air for a fairly long time, material prepared on molybdenum substrates can be peeled off and sealed into inert gas atmosphere immediately without any further treatment.

In Fig. 6.1 the spin densities N_S and average g-values of samples deposited on both aluminum and molybdenum substrates are shown. Material prepared on Al and Mo, shows the same characteristic upon decreasing I_C^{RS}. The highest N_S values are observed for the highly crystalline samples and N_S decreases monotonically with increasing amorphous phase content. However, there are some remarkable influences of the etching (HCl + H_2O) and drying process on the spin density N_S and on the average g-value. Compared to samples deposited on Mo, for material prepared on Al substrates one observes a considerable increase of N_S (Fig. 6.1 (a)) accompanied by a shift of g to higher values (Fig. 6.1 (b)). Influences can be observed for all structure compositions from highly crystalline to amorphous. The changes in N_S and the g-value are highest for material with the highest crystallinity ($I_C^{RS} = 0.81$), that also possesses the highest porosity (compare section 2.1). For highly crystalline porous material deposited on Al substrates, the spin density is a factor of three higher than compared to that deposited on Mo. The increasing N_S, from values of $N_S = 2.2\times10^{16}$ cm^{-3} (Mo substrates) to 7.2×10^{16} cm^{-3} (Al substrates), is accompanied by a shift of the average g-value from $g = 2.0044$ to 2.0046. For higher amorphous phase content the absolute changes in N_S are considerably less with $\Delta N_S \approx 10^{16}$ cm^{-3} for $I_C^{RS} = 0.71$ and they further decrease with increasing amorphous content.

To determine whether the HCl, the water, or the drying in air atmosphere causes the changes in N_S, powder obtained from samples deposited on Mo sub-

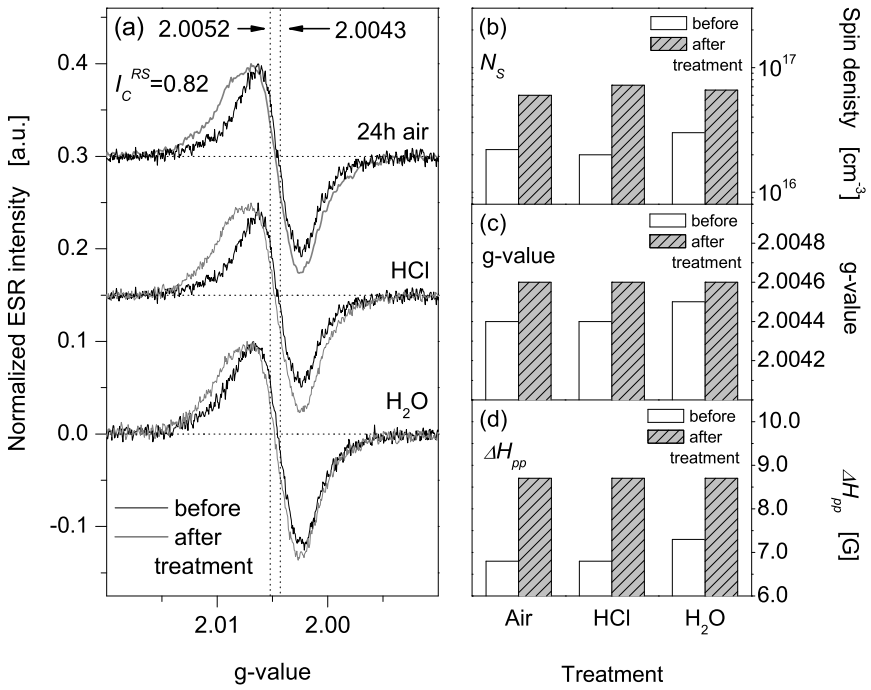

Figure 6.2: *(a) ESR spectra of highly crystalline material (I_C^{RS} = 0.82) before and after treatment in HCl, H_2O, and storage in air atmosphere. Panel (b) shows the measured values of the spin densities, (c) the g-value, and (d) the peak to peak line width ΔH_{pp} before and after treatment, respectively.*

strates was rinsed in either H_2O or HCl/H_2O solution, or was just kept in air atmosphere for 24 hours. In each case ESR spectra were recorded before and after the treatment. The results are shown in Fig. 6.2 (a). The spectra were normalized to the same peak height allowing differences in the line shape to be compared. The vertical dotted lines indicate the resonances with g-values at g=2.0043 and g=2.0052, typically observed in μc-Si:H (see section 2.2.2). Independent of the particular treatment the line shape changes significantly. The intensity of the ESR signal increases for higher g, which is equivalent with the low magnetic field site. The increase of the signal intensity at higher g-values is accompanied by a shift of the zero crossing of the ESR line towards higher values, observable in all spectra. Besides these effects, which are similar for all sample treatments discussed here, slight differences occur for the case of the H_2O treatment. Here the spectra taken before the treatment already show a higher intensity of the signal at high g-values. However, the characteristic changes upon the treatment and the observed shift of the average g-value are a general trend for all treatments. This indicates that the pre-treatment differences in the "H_2O"-spectra are a result of the fact that

instability effects already affected the material before the first measurement has been performed. This is in agreement with the observed values of the spin density N_S, the electronic g-value, and the line width ΔH_{pp} plotted in Fig. 6.2 (b, c, d). Independently of the particular treatment one observes an increase of all these three quantities. For all treatments (i) the spin density increases by up to a factor of three, saturating at values of $N_S \approx 6 \times 10^{16}$ cm^{-3}, (ii) the electronic g-value shifts to higher values starting from g=2.0044 (2.0045 for H_2O) and final values of g=2.0046, and (iii) the line width increases from $\Delta H_{pp} = 6.8 \pm 0.1$ G (7.3 ± 0.1 G for H_2O) to 8.7 ± 0.1 G. Quite surprisingly, the final values of N_S, g, and ΔH_{pp} are the same for all treatments.

This result clearly indicates that it is not the HCl etching step, which causes the additional increase in N_S, the shift of the electronic g-value, and the increased ΔH_{pp}. In fact, the observed changes are essentially the same if the powder is just treated in water and even a simple storage of the material in air leads to a similar effect. The fact that the pre-treatment values of the "H_2O"-material are slightly higher, compared to the material treated in HCl and air supports the assumption that in this case instability effects already set in before the first measurement could be performed.

The study of different treatments, described above, was performed on material with a pronounced crystallinity. The effects of an increasing amorphous phase is now discussed. For a better understanding of the results shown below, it is important to note, that with increasing amorphous content of the films the film structure may change as well as the film composition. While $I_C^{RS} = 0.82$ material shows a high degree of porosity, $I_C^{RS} = 0.71$ material is still highly crystalline, but compact. Finally $I_C^{RS} = 0.47$ material is prepared at the transition between microcrystalline and amorphous growth and shows a rather compact structure with a high a-Si:H contribution (see section 2.1).

Fig. 6.3 (a) shows the ESR spectra of material with three different structure compositions ranging from highly crystalline porous ($I_C^{RS} = 0.82$) over highly crystalline compact material ($I_C^{RS} = 0.71$) to material at the threshold between crystalline and amorphous growth ($I_C^{RS} = 0.47$). The spectra were taken before and after a H_2O treatment and then normalized in order to show differences in the line shape. Also indicated as vertical dotted lines are the resonances with g-values at g=2.0043 and g=2.0052. Changes in the shape of the ESR spectra can be observed for the $I_C^{RS} = 0.82$ and $I_C^{RS} = 0.71$ material, while on the other hand the line shape of the $I_C^{RS} = 0.47$ spectra remains unchanged upon the H_2O treatment. As for the $I_C^{RS} = 0.82$ material, which was discussed above (see Fig. 6.2), in the $I_C^{RS} = 0.71$ samples the intensity at the high g-value site of the spectra has a larger contribution to the total ESR intensity after the treatment. In Fig. 6.3 (b, c, d)

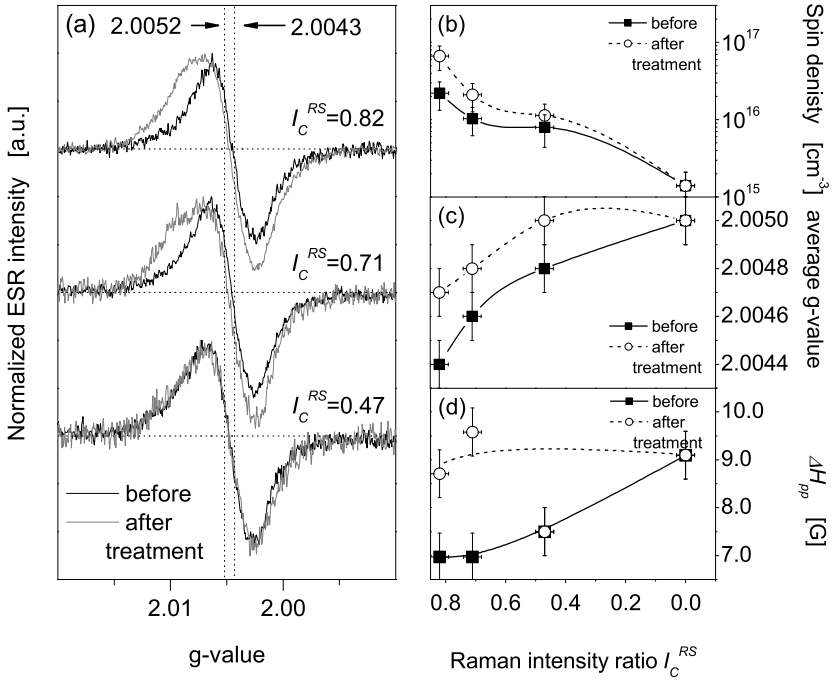

Figure 6.3: *(a) ESR spectra of material with three different structure compositions ranging from highly crystalline porous over highly crystalline compact material to material at the threshold between crystalline and amorphous growth, before and after a H_2O treatment (see section 3.3.1 for details). Panel (b) shows the measured values of the spin densities, (c) the g-value, and (d) the peak to peak line width ΔH_{pp} versus I_C^{RS}, before and after treatment.*

the absolute values of N_S, the g-value, and ΔH_{pp} versus I_C^{RS} before and after the treatment are shown. As can be seen from the figure, the magnitude of instability effects decreases with increasing amorphous phase content. While for the highest crystallinity ($I_C^{RS} = 0.82$) N_S increases by about a factor of three, the changes for the $I_C^{RS} = 0.71$ material are considerably less and almost disappear for the material prepared at the transition between microcrystalline and amorphous growth. The same effect can be observed for the values of g and ΔH_{pp}. Both quantities increase upon treatment, the absolute changes however are less pronounced for the transition material.

Because the ESR spectra of μc-Si:H can be described by two contributions at g=2.0043 (db_1) and g=2.0052 (db_2), it is interesting to see in which way and to what degree the respective spin states are involved in the increase of N_S, ΔH_{pp}, and the average g-value. The ESR spectra of Fig. 6.3 (a) therefore have been deconvoluted into these two contributions. The fits were performed using Gaussian lines with a line width of ΔH_{pp} = 5.6 G and ΔH_{pp} = 9.7 G for the db_1 and db_2

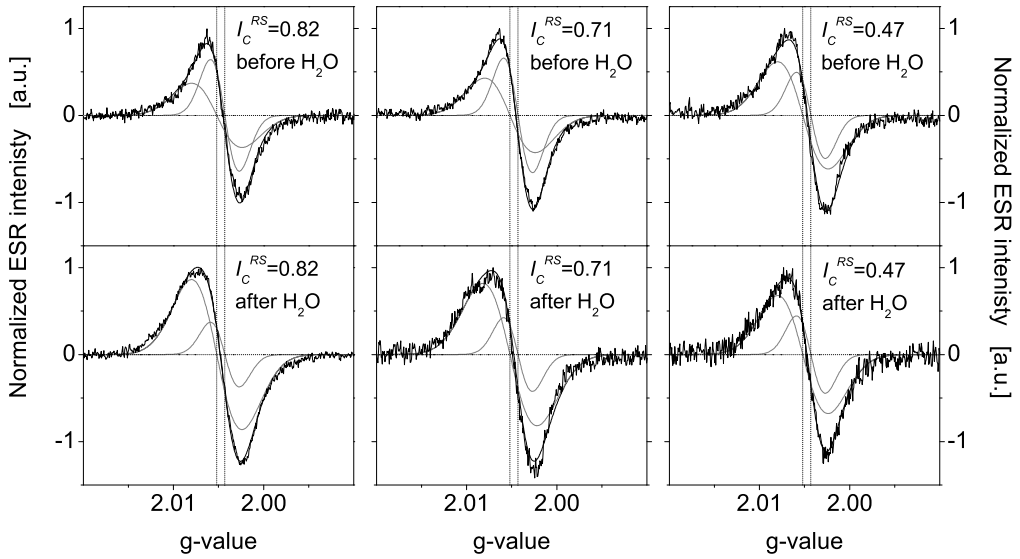

Figure 6.4: *De-convolution of the ESR spectra already shown in Fig. 6.3 (a) into the two signals at g=2.0043 and 2.0052 before (upper traces) and after the treatment (lower traces).*

resonance, respectively. For fitting, the line width and the peak position were kept fixed, and only the amplitude of the Gaussian was varied. The results are plotted in Fig. 6.4. In the figure the measured data, the fit curve as well as the individual resonances are shown. The vertical dotted lines indicate the g-values at g=2.0043 and g=2.0052. All spectra show the asymmetric μc-Si:H line shape and can be well approximated by the two resonance lines at g=2.0043 and g=2.0052. Unsurprisingly, for the transition material the relative contribution of both resonances changes only slightly. Before and after the treatment the spectra are dominated by the db_2 signal, which increases slightly after the treatment. Looking at the $I_C^{RS} = 0.82$ material the picture changes considerably. While in the original state the spectrum is dominated by the db_1 signal, the post-treated spectrum is clearly determined by spin centers contributing to the db_2 signal. The same effect, but less pronounced, can be observed for the highly crystalline but compact material. To determine the absolute changes N_S was evaluated for each resonance (db_1 and db_2) by integrating the individual fit and comparing the contributions to the total intensity of the spectra. The values of N_S determined by this procedure are shown in Fig. 6.5. The plot shows the spin density of the individual lines before and after the treatment in H_2O for each crystallinity investigated. Quite surprisingly, the treatment only effects paramagnetic states resulting in the db_2 resonance, while the line at g=2.0043 remains unaffected. For the $I_C^{RS} = 0.82$ material N_S of the

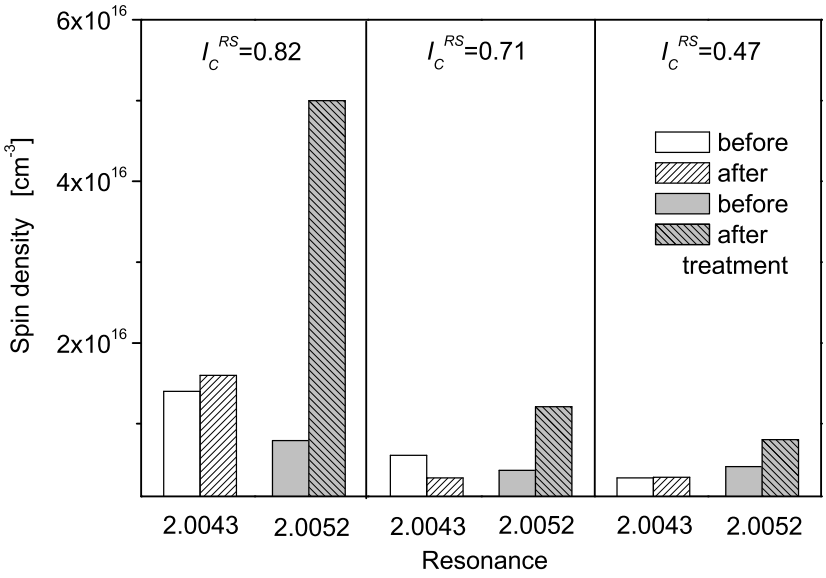

Figure 6.5: *Spin density of the resonances at g=2.0043 and g=2.0052 before and after treatment in H_2O.*

db_2 line increases by more than a factor of 6 from values of $N_S = 8 \times 10^{15}$ cm^{-3} to $N_S = 5 \times 10^{16}$ cm^{-3} while the db_1 resonance remains constant at values of about $N_S = 1.5 \times 10^{16}$ cm^{-3}. As expected from the overall spin density plotted in Fig. 6.3 (b) the absolute changes decrease with increasing amorphous content, the characteristic, however, remains the same. The line analysis shows that the increasing spin density can be attributed to an increase of the db_2 resonance while the db_1 resonance at g=2.0043 stays constant.

In this section, it has been reported that the spin density of μc-Si:H increases as a result of contact with atmospheric gases or by a treatment in H_2O. In particular, the number of spin states contributing to the db_2 resonance increases, while the spins of db_1 remain unaffected. The magnitude of the instability changes thus depends strongly on the particular structure. With increasing amorphous content and more compact structure the changes are reduced or may even disappear. However, so far the reason for these changes and the particular processes involved are unclear. It is interesting to consider if, and how, the material can be returned back to its initial state. The clear dependency of the magnitude of the changes in N_S on the structure, in particular the porosity, suggests that surface processes are involved. Assuming that the changes in the ESR signal intensity are a result of adsorption of atmospheric gases or water, annealing in inert gas atmosphere or vacuum might restore the initial material properties. This is the subject of the

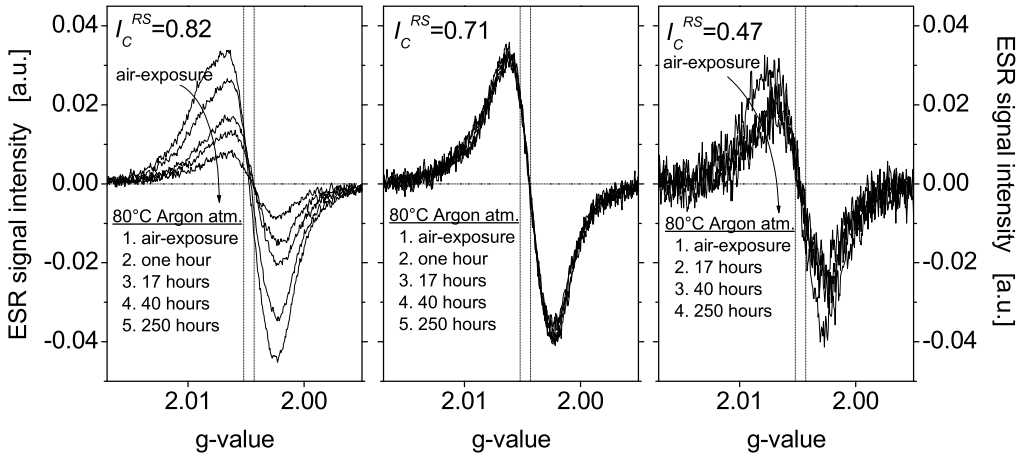

Figure 6.6: *ESR signals of highly crystalline porous ($I_C^{RS} = 0.82$), highly crystalline compact ($I_C^{RS} = 0.71$), and from material at the transition from crystalline to amorphous growth ($I_C^{RS} = 0.47$ for different annealing periods.)*

following section.

6.1.2 Reversible Effects in the ESR Signal

Material as studied above, i.e. with structure compositions including highly crystalline porous, highly crystalline compact, and transition material with a considerable amount of a-Si:H phase, has been stored in air for a prolonged period and afterwards sealed into argon atmosphere. The samples were then annealed at a temperature of 80°C for several hours. At regular intervals the annealing process was interrupted in order to measure ESR. The resulting spectra are plotted in Fig. 6.6. Unlike the ESR measurements shown before, these spectra are not normalized to the same peak height, but relative to the initial curve, denoted as (1.). Again the vertical lines indicate the position of the g-values at g=2.0043 and g=2.0052.

The most outstanding result in Fig. 6.6 is that quite moderate annealing temperatures of $T = 80$°C strongly influence the ESR signal. As expected from the instabilities observed above, the magnitude of the effects is closely connected to the structure of the material. Significant changes can be observed for the highly crystalline porous material ($I_C^{RS} = 0.82$). The ESR signal decreases strongly after one hour annealing in argon atmosphere. With increasing annealing period t_{ann} the signal intensity decreases further. On the other hand, the ESR signal of the highly crystalline compact material ($I_C^{RS} = 0.71$) changes only slightly. This is quite surprising as instability effects could also be observed for these types of

sample[1] (see Fig. 6.3). Looking at the initial spectra of this sample, one can not see the typical shoulder at the high g-value site, expected for material exposed to air or water. The reason for the quite constant resonance upon annealing might therefore be a result of a higher stability of the material upon treatment in air or water. The transition material ($I_C^{RS} = 0.47$) shows the same behavior like the $I_C^{RS} = 0.82$ material. The ESR signal intensity decreases after annealing in argon atmosphere at $T = 80°C$. As expected from the instability results described in section 6.1.1 the effect is less pronounced, compared to the highly crystalline porous material.

As already mentioned above, the decreasing ESR signal intensity directly scales with N_S. In fact, from Fig. 6.6 it is clear that the spin density decreases for the $I_C^{RS} = 0.82$ and 0.47 material, as a function of annealing period t_{ann}. While the increase of the spin density exposure to air or water has been attributed to an increase of the number of spins with a g-value of g=2.0052, the annealing also just affects the db_2 resonance. This is shown in Fig. 6.7 (a, b), where the spin densities of the individual resonances db_1 and db_2 are plotted versus t_{ann}. Except for the $I_C^{RS} = 0.71$ material, N_{db_2} decreases, while N_{db_1} remains constant. The decrease of the spin density at g=2.0052 is accompanied by a shift of the average g-value and a decrease of the line width ΔH_{pp}. Both quantities are plotted in Fig. 6.7 (c) and (d), respectively. For the $I_C^{RS} = 0.82$ material, annealing for 250 hours the spin density decreases from 4×10^{16} cm^{-3} to 9×10^{15} cm^{-3}, while the average g-value shifts from 2.0047 to 2.0044 and line width decreases from $\Delta H_{pp} = 8.8$ G to 7.6 G. The final values after 250 hours annealing in argon atmosphere at 80°C are close to the initial values of the material before the exposure to air, as can be seen from Fig. 6.3 and 6.5. In fact, the increase of the spin density N_{db_2}, the shift of the g-value, and the increase of the line width ΔH_{pp} can be reversed by a simple annealing step in argon atmosphere at temperatures of $T = 80°C$. Interestingly, the reversible behavior in the ESR signal, particular the strong changes found in $I_C^{RS} = 0.82$ material upon air-exposure and annealing can be repeated many times without any sign of fatigue.

However, while the spin density decreases upon annealing the question arises at what point the decrease will saturate. After 250 hours N_S shows an asymptotic behavior, but still does not saturate. Assuming the involved processes are thermally activated an increase of the temperature might accelerate the procedure. Annealing/air-exposure cycles have therefore been performed at a temperature of $T = 160°C$. The temperature was carefully chosen to considerably activate the process without leading to a desorption of hydrogen, which in term would lead to the creation of additional dangling bond defects. Fig. 6.8 shows the results

[1] Note, that the samples used for annealing are not the same as the once used for the treatments in H_2O. However, the particular deposition parameters have been kept constant.

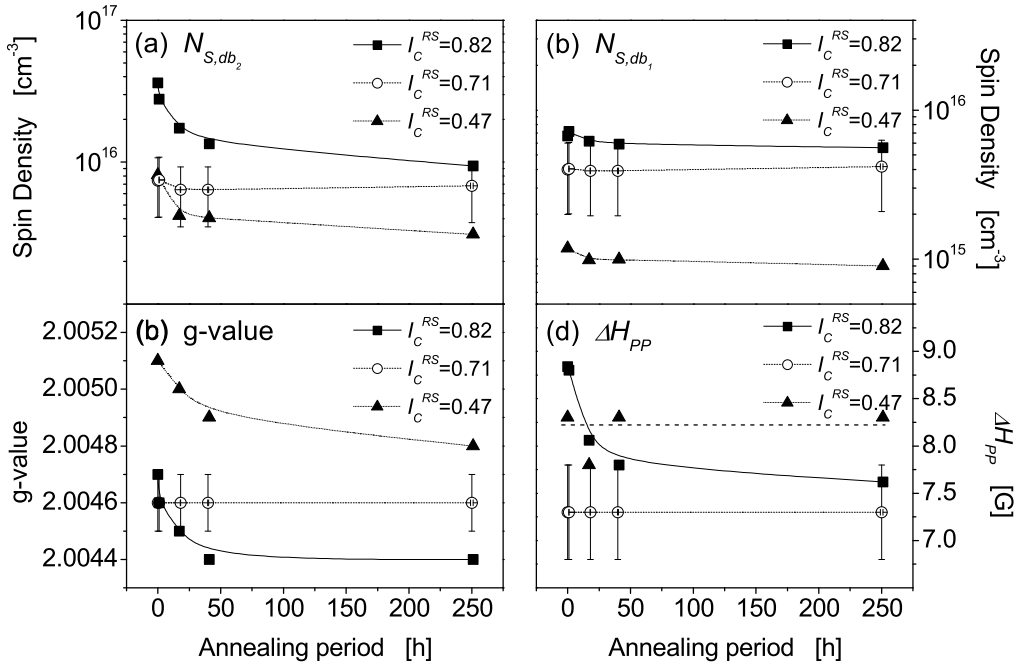

Figure 6.7: *The absolute values of N_S for the individual lines at (a) g=2.0052 and (b) g=2.0043 were determined by deconvoluting the spectra shown in Fig. 6.6. In panel (c) and (d) the extracted values of g and ΔH_{pp} are plotted versus the annealing period.*

obtained from annealing the highly crystalline porous material ($I_C^{RS} = 0.82$) in argon atmosphere. For the experiment the sample was stored in air for about 50 hours (upper trace in Fig. 6.8). After annealing the material at $T = 160°C$ for one hour, the ESR spectrum as shown as the middle trace in Fig. 6.8 was recorded. Quite surprisingly, the spectrum shows a strong contribution of the conduction electron resonance, after annealing (compare section 2.2.2). This suggests a considerable shift of the Fermi level up into the conduction band-tail. To determine N_S of the individual lines, the spectra were deconvoluted as indicated by the gray lines, shown in Fig. 6.8. The spin densities of the two resonances at g=2.0043 and g=2.0052 decrease as a result of the annealing. The particular values are plotted in table 6.1. The high number of electrons trapped in conduction band-tail states ($N_{CE} = 6 \times 10^{16}$ cm^{-3}) suggests a considerable background doping in this sample. Quite surprisingly, these changes are reversible and the material can be treated back to its initial state by simply exposing it to air atmosphere, as shown in the lower trace of Fig. 6.8.

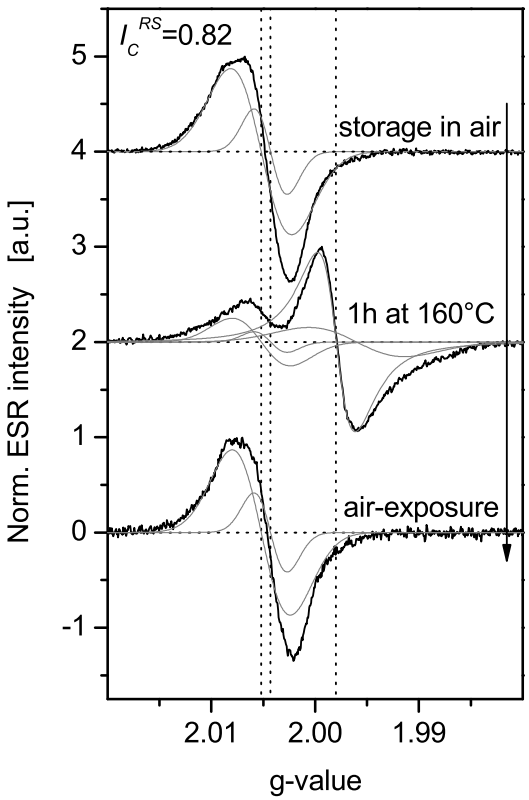

Figure 6.8: *ESR signal of highly crystalline porous μc-Si:H after storage in air (upper trace), after annealing at T = 160°C for one hour (middle trace), and after an additional air-exposure. The vertical dotted lines indicate the g-values of g=2.0043 and g=2.0052 and g=1.998.*

6.1.3 Reversible Effects in the Electrical Conductivity

The changes in the ESR signal described above suggest that reversible effects might also affect the electrical transport. In particular, the emergence of a strong CE signal after annealing the highly crystalline porous material at elevated temperatures (see Fig. 6.8) suggests considerable shifts of the Fermi level, which might also be visible in the electrical conductivity. Fig. 6.9 shows a temperature cycle taken after the material was stored in air atmosphere for about one week. The samples were measured in a temperature range between T = 100K and 450K (•). The material was than kept in vacuum and annealed for 6 hours at $T = 450K$. Afterwards the dark conductivity $\sigma_D(T)$ has been measured again (△) in the temperature range between T = 450K and 100K. Reversible effects as a result of air-exposure and annealing cycles, as observed in ESR, can also be seen in σ_D. The dark conductivity of I_C^{RS} = 0.82 material, shown in Fig. 6.9 (a), shows

Table 6.1: Spin densities of the individual resonances of the $I_C^{RS} = 0.82$ material after air-exposure and followed by annealing for one hour at 160°C in argon.

Resonance	N_S (storage in air)	N_S (after annealing)	N_S (air exposure)
g=2.0043	1×10^{16} cm^{-3}	2×10^{15} cm^{-3}	1×10^{16} cm^{-3}
g=2.0052	5×10^{16} cm^{-3}	1×10^{16} cm^{-3}	5×10^{16} cm^{-3}
g=1.998−1.996	–	6×10^{16} cm^{-3}	–

considerably lower values after contact with air, over the entire temperature range investigated. After exposing to air the room temperature conductivity decreases by more than one order of magnitude. The conductivity can be restored to its initial values by annealing the material, just like for the changes observed in ESR. However, there is a distinct difference of the electrical dark conductivity σ_D between the porous and compact highly crystalline material upon storage in air and annealing steps. As for the highly crystalline porous sample ($I_C^{RS} = 0.82$) the room temperature dark conductivity decreases after storage in air, one can observe the opposite for the compact material, as shown in Fig. 6.9 (b). For the $I_C^{RS} = 0.71$ material the dark conductivity increases upon contact with air. Material prepared at the transition between microcrystalline and amorphous growth does not show any changes upon contact with air or annealing. Again the air-exposure/annealing cycles can be repeated many times without any sign of fatigue. The observed

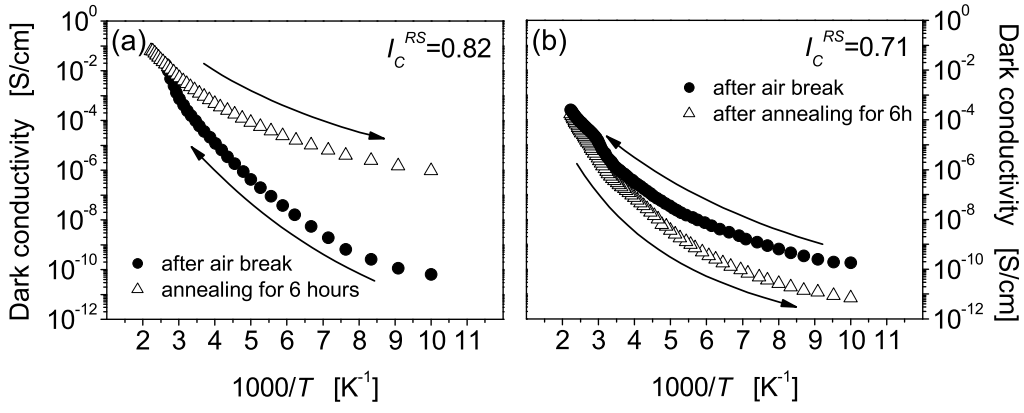

Figure 6.9: *Dependence of the temperature dependent dark conductivity $\sigma_D(T)$ on annealing/air-exposure cycles of (a) highly crystalline porous and (b) highly crystalline but compact material.*

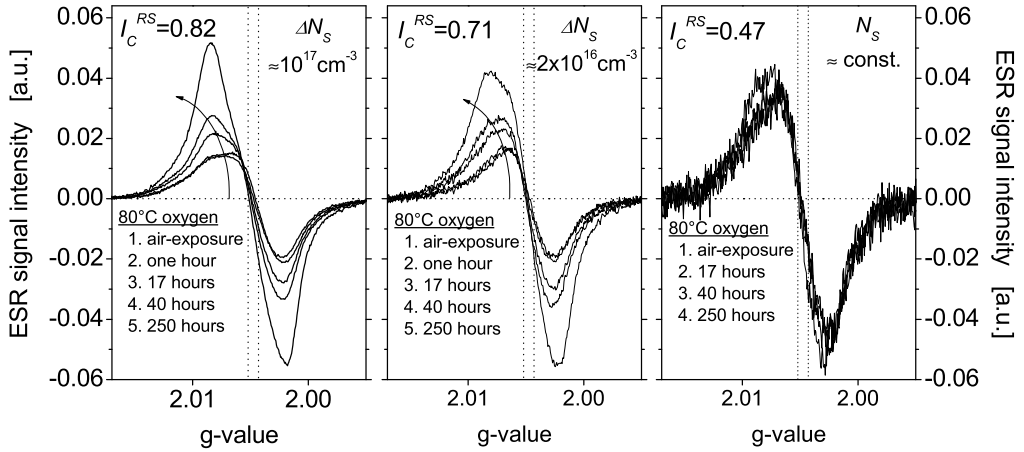

Figure 6.10: *ESR signals of highly crystalline and porous ($I_C^{RS} = 0.81$), highly crystalline compact ($I_C^{RS} = 0.72$), and of material at the transition from crystalline to amorphous growth ($I_C^{RS} = 0.47$)*

reversible effects in σ_D show many similarities to earlier investigations made on material which was grown using the chemical transport technique [20] or hot wire chemical vapor deposition [166].

6.2 Irreversible Oxidation Effects

As shown above, storing highly crystalline μc-Si:H in air atmosphere results in a reversible increase of the spin density accompanied by a shift of the average g-value. However, it has been shown by e.g. infrared spectroscopy, that highly crystalline μc-Si:H is also susceptible to oxidation effects [11, 20, 51, 13], forming Si-O bonds at the grain boundaries, which are stable up to temperatures of T = 1050 K [20]. In the following section, effects of the oxidation of the grain- or column boundaries on the ESR signal will be studied. Therefore, samples with different structure compositions, in fact material prepared in the same run as the one used for the air-exposure/annealing cycles (section 6.1), have been sealed into oxygen atmosphere and annealed at temperatures of $T = 80°C$. After selected time intervals the annealing process was interrupted and ESR spectra were recorded. The spectra measured for the three structure compositions are shown in Fig. 6.10. As for the reversible changes discussed above, the magnitude of the observed changes strongly depends on the structure composition of the μc-Si:H. However, in contrast to the treatment in argon, annealing in oxygen atmosphere at a temperature of T = 80°C leads to an increase of the ESR signal intensity. The observed line shape of the resonance differs significantly from that

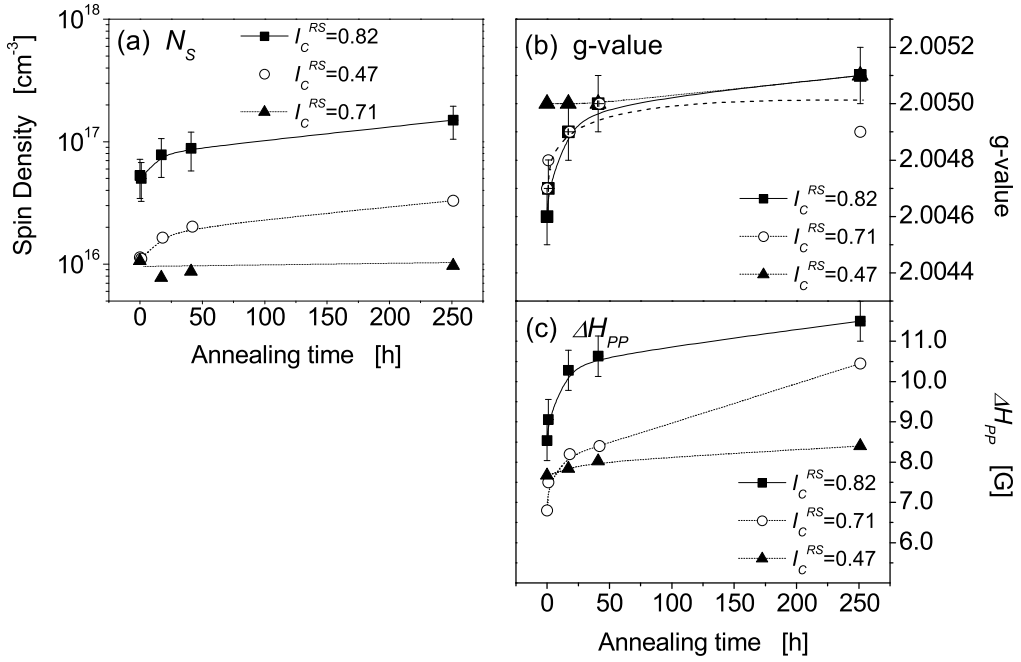

Figure 6.11: *Absolute values of (a) the spin density, (b) the g-value, and (c) the peak to peak line width as a function of the annealing period.*

observed in μc-Si:H. In fact, it is impossible to fit the measured data with any combination of the two resonances at g-values of g=2.0043 and g=2.0052. Fitting with three resonance lines might appear promising, but cannot be justified without more experimental evidence. On the other hand, a fit with three signals (either Gaussian or Lorentzian) using as many as 9 free parameters (peak position, width, amplitude for each signal) is most questionable. The absolute values of N_S, g, and ΔH_{pp} shown in Fig. 6.11 are therefore extracted from the overall signal without deconvoluting the spectra. The spin density, plotted in panel (a), increases with increasing annealing period. The changes are highest for the highly crystalline porous material ($I_C^{RS} = 0.82$), where the overall N_S increases from values of $N_S(t = 0) = 5 \times 10^{16}$ cm^{-3} to $N_S(t = 250h) = 1.5 \times 10^{17}$ cm^{-3}. With increasing amorphous content the porosity of the material and therefore the active surface area decreases. The increase of N_S within 250h is less pronounced, with $\Delta N_S \approx 2 \times 10^{16}$ cm^{-3} for $I_C^{RS} = 0.71$ material, or even disappears for $I_C^{RS} = 0.47$. The increase in the spin density is accompanied by a shift of the average g-value, which is shown in Fig. 6.11 (b). Again the changes are highest for the porous sample where the g-value increases from g=2.0046 to g=2.0051; the shift becomes less pronounced upon increasing amorphous content. As can be seen in Fig. 6.10, while the oxidation process proceeds, the peak to peak line width of

the overall signal increases. The absolute values, plotted in Fig. 6.11 (c), confirm that the magnitude of the changes strongly depends on the structure of the material. While for the porous material the line width increases from values of ΔH_{pp} = 8.5 G to 11.5 G, ΔH_{pp} of the transition material increases only slightly.

In contrast to the air-exposure/annealing cycles described in section 6.1, annealing of oxidized samples in argon at temperatures below $T = 200°C$ does not have any effect on the ESR signal. For higher temperatures than $T = 200°C$ bonded hydrogen, used to terminate vacant Si bonds, will desorb, resulting in a further increase of the dangling bond density. However, assuming that the increasing spin density, observed in Fig. 6.11, is a result of the oxidation, a dip into hydrofluoric acid (HF), well known from silicon wafer cleaning technology, provides a simple way to remove the oxide from the surface and by the way passivating dangling bonds by establishing Si-H bonds.

6.2.1 Reversibility by Chemical Reduction

In order to remove the oxygen surface layer a 5% HF solution was used. The sample was etched in the acid for 30 seconds, carefully rinsed in distilled water, and dried by flushing with nitrogen. To avoid as much re-oxidation and post-contamination as possible the sample was immediately sealed in argon atmosphere and measured within 5 min after the cleaning process. For the ease of sample handling material has been prepared on glass substrates. The price to pay is a considerably lower signal to noise ratio due to the reduced sample volume. Additionally, the ESR spectra of the μc-Si:H is superimposed by signal traces from the borosilicate glass at g=2.001. However, still one can easily observe the effects as shown in Fig. 6.12 (a). The figure shows three spectra of highly crystalline porous material (i) taken right immediately after the deposition, (ii) after an annealing step in O_2 atmosphere for two hours at $T = 160°C$, and (iii) after the treatment in HF acid. The spectra shown are not normalized, so differences in the signal intensity are a result of a change in the spin density. After annealing in O_2 atmosphere for two hours the spectrum shows a higher intensity compared to the "as deposited" signal, indicating an increase of N_S. In fact, the spin density increases from values of $N_S = 5 \times 10^{16}$ cm^{-3} to $N_S = 2 \times 10^{17}$ cm^{-3}, resulting in the same line shape as observed for the O_2-annealed material in Fig. 6.10. After the HF-dip the intensity decreases again and the line shape returns back to its initial form. Looking at the absolute values of N_S, the g-value, and ΔH_{pp}, plotted in Fig. 6.12 (b, c, d) the success of the HF-dip becomes more obvious. While all three quantities increase after annealing in oxygen, which in fact is the same effect as observed for the powder samples, all three quantities restore back to their initial values, after the treatment in HF acid.

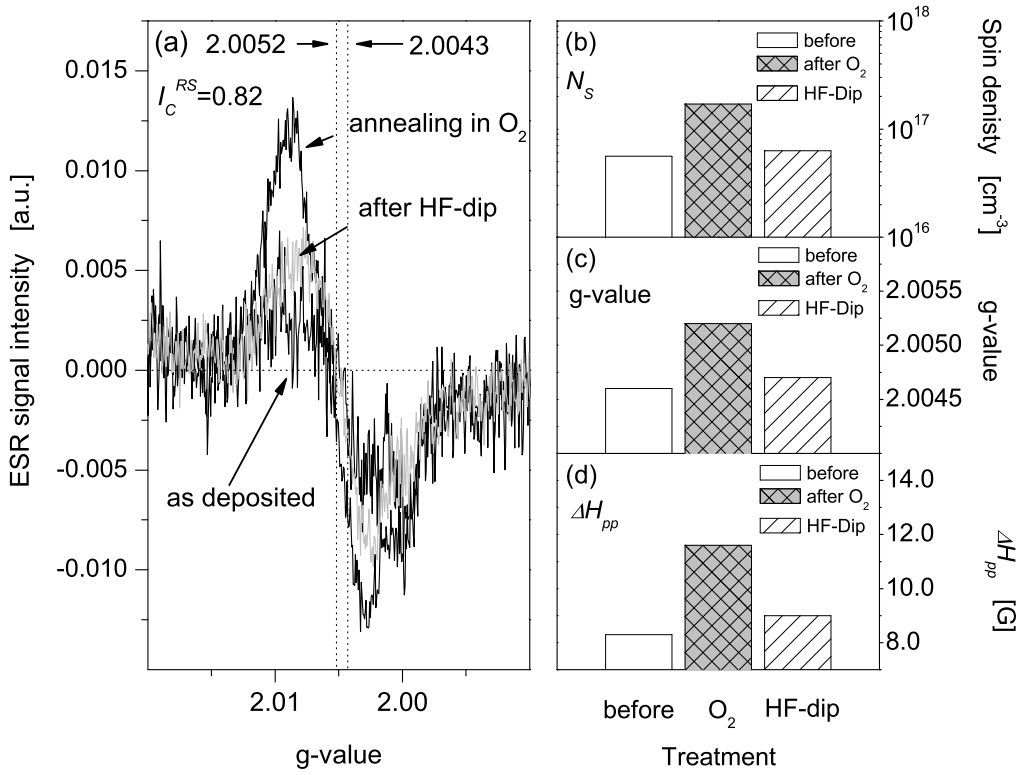

Figure 6.12: *(a) ESR spectra of a porous μc-Si:H sample (I_C^{RS} = 0.82) deposited on glass substrate measured right after deposition, annealing in O_2, and after etching in HF. In panel (b) the measured values of N_S, (c) the g-value, and (d) ΔH_{pp} before and after the HF-dip are shown.*

6.2.2 Charge Transfer caused by Oxidation of N-Type μc-Si:H

As shown above, annealing μc-Si:H in oxygen atmosphere leads to an increase of the spin density. The fact that the corresponding resonance appears at higher g-values and exhibits a different line shape than observed for the resonances at g=2.0043 and g=2.0052 suggests that the additional spin states are somehow different. In Chapter 5 the use of phosphorous doping to probe the density of gap states was described and it was found that the shift of the Fermi level is governed by the compensation of gap states. In fact, states within the band gap have to be filled before states in the conduction band-tail can be occupied.

The aim of this section is to use the n-type doping experiment just in the opposite direction. The question is, if and how the spin states created by the oxidation of the surface affect the position of the Fermi level and lead to a depopulation of conduction band-tail states. Annealing experiments have therefore

been performed on $I_C^{RS} = 0.82$ material with phosphorous doping concentrations of 10^{17} cm^{-3}. The highly crystalline porous material was chosen because it showed the biggest changes upon oxidation (see Fig. 6.10). The measured spectra taken after different stages of the oxidation process are shown in Fig. 6.13 (a). In the initial state the ESR signal is dominated by the CE resonance, which arises from electrons trapped in conduction band-tail states. As expected from the experiments on intrinsic material the intensity of the ESR signal around g=2.005 increases as a function of the annealing period. With the creation of additional states, the CE centers become depopulated resulting in a decrease of the signal intensity around g=1.998. This will happen when the states created by the oxidation are located lower in energy than the CE states. Providing that these states can accommodate additional electrons they will become occupied, while states in the conduction band become depopulated. The assumption that the electrons are transferred from CE states to states created by oxidation of the surface is supported by absolute values of the spin density plotted in Fig. 6.13 (b). The spin density was determined by integrating the ESR spectra over the entire range measured. It is surprising, that

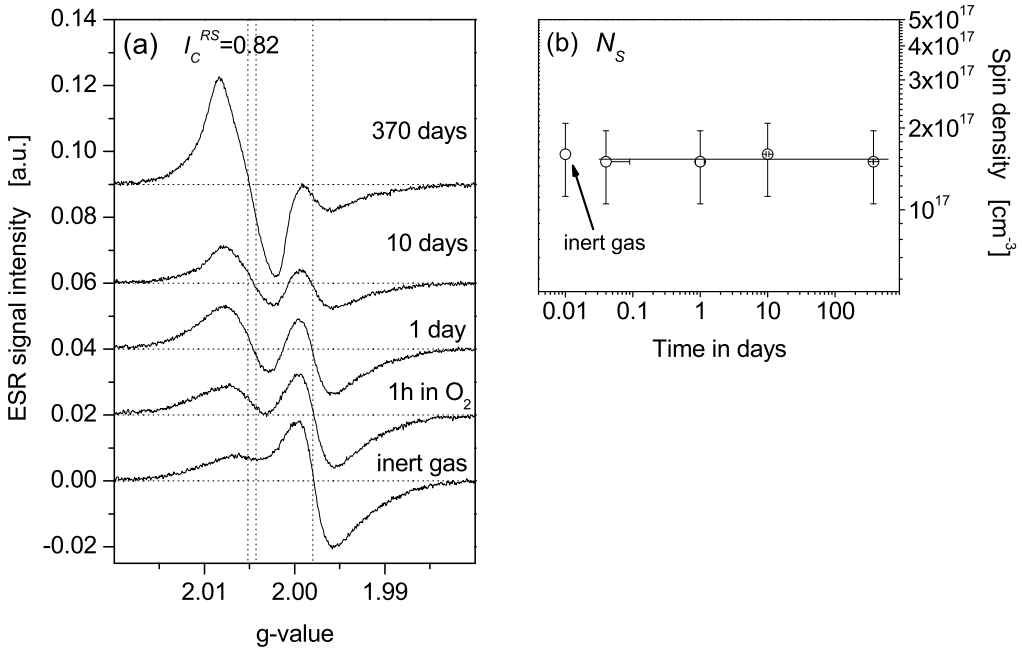

Figure 6.13: *ESR signal of a n-type highly crystalline porous μc-Si:H sample with 10 ppm PH_3 doping for different periods of storage in oxygen atmosphere. The measurements were taken at T = 40K. In (b) the number of spins (N_S), contributing to the spectra shown in panel (a) is shown; the spectrum taken in inert gas is arbitrarily set at 0.01 days.*

upon annealing the total number of spins observed in ESR does not vary, while the g-value changes considerably. As the value of g is strongly connected to the microscopic environment surrounding the paramagnetic state, this indicates that only the microscopic location of the resonant electrons changes and defect states created by oxidation are not involved in compensation effects. The reason for this remains unclear and requires further investigation.

6.3 On the Origin of Instability Effects in μc-Si:H

In- and out-diffusion of impurities and atmospheric gases leads to numerous instability and metastable phenomena on the ESR signal and the electrical conductivity in μc-Si:H at or close to room temperature. It appears, that the amplitude of these changes is connected to the surface area of the material. Reversible and irreversible changes in N_S are highly pronounced for $I_C^{RS} = 0.81$ material which exhibit a very porous structure (compare section 2.1). In highly crystalline material with only a minute amount of amorphous phase content, which has shown to be compact, the effects are much less prominent and are almost absent for still lower I_C^{RS}. In the following section the observed meta-stable and irreversible effects in μc-Si:H of various structure compositions will be discussed. The main effects to consider are adsorption and oxidation on surfaces, caused by atmospheric gases.

6.3.1 Adsorption of Atmospheric Gases

The results presented in section 6.1 show that the spin density N_S, the average g-value, as well as the electrical conductivity σ_D strongly depend on the particular treatment and the history of μc-Si:H material. While N_S increases upon storing in air atmosphere, the effect can be reversed by a simple annealing step in argon atmosphere. A detailed analysis of the ESR spectra shows that the changes in N_S can be traced back to a varying number of spins with a g-value of g=2.0052, while the db_1 resonance at g=2.0043 remains unaffected. On the other hand, for σ_D not only the amplitude, but also the direction of the changes depends on the structure of the material. While for the $I_C^{RS} = 0.82$ material σ_D decreases, an increase is observed for the $I_C^{RS} = 0.71$ material as a result of a storage in air atmosphere. The airbreak/annealing cycles can be observed still after many cycles with no fatigue or the appearance of any irreversible effect.

The question arises, how far the observed effects of the various structure compositions can be related to each other and/or have the same origin. Taking into account the low energies required for the air-exposure/annealing cycles one can exclude the possibility of breaking up and annealing of Si-DB as a possible origin for the varying N_S. One could also speculate that adsorption leads to a strong

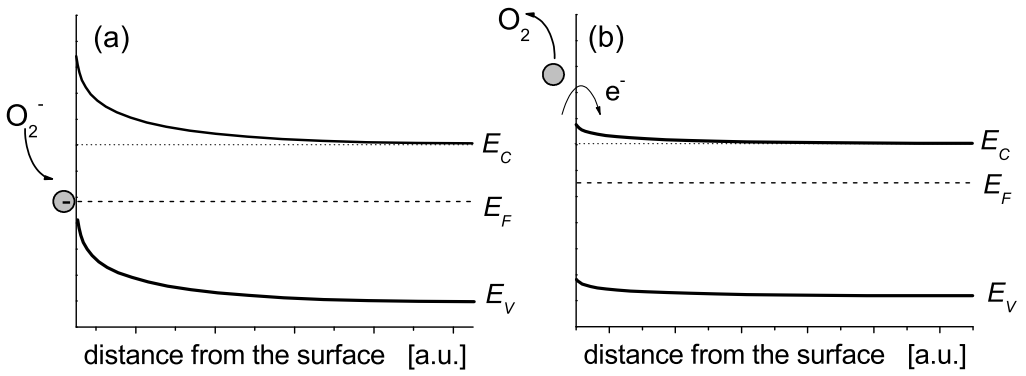

Figure 6.14: *Energy band bending and Fermi level shift due to (a) the adsorption and the (b) desorption of oxygen on surface of μc-Si:H.*

band bending, which could result in a bond breaking via weak-bond dangling bond (WB-DB) conversion, similar to the field effect and doping induced defect creation found in a-Si:H [167]. However, it is difficult to fit the reversibility of the observed effects with the WB-DB conversion. Taking the reversible changes of σ_D into account, the adsorption of oxygen seems to be a most likely candidate [20] to explain the observed metastable effects in ESR and electrical conductivity. In fact, while the material is in contact with air, additional surface states can arise due to the adsorption of atmospheric gases. The following models have been mainly developed and have widely been used to explain the gas sensing properties of semiconducting oxides, like SnO_2 and ZnO [168, 169, 170, 171, 172].

As determined by Hall measurements, for intentionally undoped μc-Si:H one generally observes n-type behavior. The in-diffusion of oxygen along the column boundaries and the adsorption of O_2 on the surface of the crystalline columns will therefore capture an electron from the conduction band forming an O_2^- state. The capturing of the electron is equivalent to the occupation of a localized surface state, induced by the adsorption of O_2. This is possible, because the energy level of the O_2^- state is below the Fermi level of the material without the presence of oxygen. This can be described by the following reactions

$$\begin{aligned} &O_{2(gas)} \Rightarrow O_{2(ads)} \\ &e^- + O_{2(ads)} \Rightarrow O^-_{2(ads)}. \end{aligned} \tag{6.1}$$

The transfer of charge carriers will lower the Fermi level and the accumulation of trapped charge carriers at the column boundary will lead to a band bending in the material. This is shown schematically in Fig. 6.14. The changes of the dark conductivity σ_D are therefore a result of two different, however interconnected effects. While the trapping of charge carrier at the surface leads to changes in

the free carrier concentrations, the increasing barrier height handicaps the charge carrier transport. As dark conductivity in μc-Si:H is usually measured perpendicular to the growth direction, a charge carrier has to cross a number of column boundaries before it reaches the other electrode (compare Fig. 2.1). To overcome the barriers formed at the column boundaries, a charge carrier has to be thermally excited. This model of barrier-limited transport is based on the ideas of Seto [41] and has been successfully applied to explain the transport behavior of polycrystalline silicon. In the case that the free charge carrier concentration in the columns is higher than the density of surface states induced by adsorption of O_2 the current is given by

$$I = const \cdot \exp\left(\frac{-E_B}{kT}\right) \tag{6.2}$$

and is so extremely sensitive to the barrier hight E_B. This assumption is plausible if one bears in mind that a typical surface adsorption will exchange charge carriers of the order of $10^{10} - 10^{12}$ e/cm^2 [173]. Taken a charge carrier concentration of $N_D = 10^{17}$ cm^{-3} in the bulk of μc-Si:H [96] and a column diameter of 200 nm the free charge carrier concentration is about one order of magnitude higher than the number of surface states created by adsorption. Upon annealing in argon atmosphere, the desorption of oxygen will lead to a re-emission of the trapped charge back into the bulk. The band bending will decrease to its initial state and restoring the values of the electrical conductivity.

The considerations made above can explain the reversible effects observed in highly crystalline porous material $I_C^{RS} = 0.82$ very well. For highly crystalline but compact material $I_C^{RS} = 0.71$, on the other hand, the conductivity shown in Fig. 6.9 strongly deviates from the characteristic found in $I_C^{RS} = 0.82$ material. While for the later one σ_D decreases, for $I_C^{RS} = 0.71$ material σ_D increases upon contact with air.

The key-issue for the different behavior is the porosity. While in highly crystalline porous material atmospheric gases can easily diffuse along the column boundaries leading to the creation of surface states, the compact structure of $I_C^{RS} = 0.71$ prevents the diffusion of atmospheric gases into the material. One would therefore not expect any strong influence on the barrier height at the column boundaries upon contact with air atmosphere. However, oxygen can still be adsorbed at the film surface. Providing that the charge carrier density within the film is small, i.e. the Fermi level position is close to the mid gap, the creation of O_2^- states at the film surface might lead to the induction of holes. In fact, due to the capture of an electron by the surface state, holes are induced into the film, resulting in an increasing σ_D. Adsorption processes could therefore also account for the meta-stability of σ_D in highly crystalline compact material. This assumes that the O_2^- surface states lies energetically below mid gap, which however re-

mains speculative. However, this process was recently suggested to account for the properties of porous silicon gas sensors [174].

Can this adsorption process, as described above, also account for the reversible effects found in the ESR signal? Caused by the band bending, states located in surface near regions become depopulated. The particular details are difficult to predict as they will depend on the relationship between the effective correlation energy, the energy position and the energy distribution of the defects. In a simple picture, if one starts from a negatively charged D^- state, depopulation will lead to a neutral D^0 state and one would observe an increase of the ESR signal intensity. Upon annealing in argon atmosphere, the desorption of oxygen will lead to a re-emission of the trapped electrons back into the film restoring the initial values of N_S.

Compatible with the change in occupation of near-surface states is the effect of annealing at 160°C in Ar. In highly crystalline porous material ($I_C^{RS} = 0.82$) this leads to the appearance of a strong CE signal, resulting from a shift of the Fermi level into the conduction band-tail (compare Chapter 5). The observation is in agreement with the direction and magnitude of changes observed in σ_D and indicates considerable n-type background doping of this nominally un-doped sample. A comparison with the data measured in Chapter 5 the magnitude of the CE resonance will correspond to a doping concentration of about $N_D \approx 7$ ppm. Because of the reversibility of these effect upon contact with air, one can exclude thermally induced dopant activation as the dominating process. However, the reason for this strong shift of E_F in $I_C^{RS} = 0.82$ material remains yet unknown.

It is interesting, that the changes in N_S are due to an increasing number of spin states at g=2.0052 while the resonance at g=2.0043 remains unaffected. The data suggest that both states, db_1 and db_2, are located in different microscopic environments, spatially separated from each other. In fact, from the study of intrinsic μc-Si:H material, it was concluded that the db_2 signal arises from states located at the column boundaries, while on the other hand, there are some indications that the db_1 is connected to the crystalline grains. Taking into account a Debye screening length of

$$L_D = \sqrt{\frac{\varepsilon\varepsilon_0 kT}{N_D q^2}} \approx 12.5 \text{ nm} \tag{6.3}$$

and a diameter of the columnar clusters of 200 nm, the observed processes are restricted to the surface of the crystalline columns. In other words, the depopulation of D^- states, caused by the band bending upon contact with air, only occurs in regions close to the surface. Because the increasing ESR signal intensity is borne by the db_2 states, it is tempting to relate the db_2 signal to states located at the columnar surface. On the other hand, the fact that the db_1 states remain unaffected by

the treatment suggest that they are located within the crystalline columns.

6.3.2 Irreversible Effects caused by Oxidation

Unlike the reversible adsorption effects, the effects of oxidation on the ESR signals are not reversible by moderate temperature annealing or long time storage in inert gas or in vacuum. The process seems to be thermally activated, starting already at room temperature. The non-reversible occurrence of additional spins by annealing in oxygen is linked to this oxidation process. The effect is again closely related to the size of the surface area and the fact that the increase of N_S after annealing in O_2 or air can be restored by an HF dip supports that the observed effect is a surface process. The depopulation of CE states due to creation of Si-O related defect states supports the assumption that the energy of additional states observed in ESR is below the energy of conduction band-tail states. In this context, it is remarkable that electrons located in conduction band-tail states seems to be transferred to states created by oxidation and are not involved in compensation effects, as reported in Chapter 5. However, more evidence from experimental data are need to resolve this issue. Infrared as well as secondary ion mass spectroscopy combined with ESR and electronic conductivity of material in various oxidation states seems a promising task for the future.

6.4 Summary

The instability and metastability phenomena in μc-Si:H are numerous and are a matter of great concern for the understanding of the material properties as well as for possible technological applications of these materials. It appears, that the amplitude of these changes is connected to the surface area of the material. N_S changes due to adsorption are highly pronounced for $I_C^{RS} = 0.81$ material, which is known to be very porous. At lower I_C^{RS} the effects are much smaller or absent. With increasing amorphous content the material is getting more compact and the additional amorphous phase, incorporated between the crystalline columns, leads to a better termination of the crystal surfaces, which are therefore less susceptible for adsorption of impurities and atmospheric gases. Note, that the optimum μc-Si:H material for solar cells is found close to growth conditions of amorphous material. The fact, that the changes only affect the db_2 resonance (g=2.0052) supports an earlier assumption that the related defect is separated from the defect resulting in the db_1 line (g=2.0043). Most likely, the db_2 defect is located at or near the grain boundaries, while the db_1 states is located within the crystalline columns. An alternative explanation for the increase of the db_2 resonance would relate the resonance with states of the adsorbed species.